Thermocapillary suppression of the Plateau–Rayleigh instability: a model for long encapsulated liquid zones

By Y.-J. CHEN[1], R. ABBASCHIAN[2] AND P. H. STEEN[3]

[1]454 Corporation, 20 Commercial Street, Branford, CT 06405, USA

[2]Department of Material Science and Engineering, University of Florida, Gainesville, FL 32611, USA

[3]School of Chemical Engineering and Center for Applied Mathematics, Cornell University, Ithaca, NY 14853, USA

A cylindrical liquid bridge is unstable when its length is longer than its circumference, the Plateau–Rayleigh limit. This capillary instability is modified by fluid motions adjacent to the interface, which can be induced by thermocapillary stress, among other means. A simple flow model with symmetry that mimics the situation in encapsulated floating zones is analysed. The interfacial balance equation is formulated as a bifurcation problem, appropriate when the flows are nearly rectilinear. This balance captures the competition between capillary stress and the flow-induced pressure. The fluid motions are shown to have a stabilizing effect; bridges much longer than the classical limit are stabilized. Numerical branch-tracing and the Lyapunov–Schmidt reduction methods provide the bifurcation structures of branching solutions. A normal-form analysis predicts standing-wave patterns due to mode–mode interaction. The model is proposed as an explanation for the extra long float zones observed in various spacelab experiments.

1. Introduction

In space shuttle experiments on float-zone crystal growth, the molten zones are created by subjecting a cylindrical sample of solid material to a ring heater. The liquid bridge thereby created is hot in the middle (midplane) and cooler away from the heater. Far enough away from the midplane, the liquid zone is bounded by the solid unmelted material. Variation of the temperature along the liquid interface results in a thermocapillary stress that drives fluid motion in the liquid. Several experiments show that bridges may be longer than the Plateau–Rayleigh (PR) limit. From an early flight (STS-41D; 1984) came a qualitative report of float-zone length nearly twice the PR limit (Murphy *et al.* 1987). These authors suggested that a thin oxide layer of high-melting-point material may have formed on the interface and may have thereby acted as a tubular container. Measurement of the layer thickness was not possible. During a more recent flight (STS-57; 1993), there were again observations of extra-long float zones, with lengths reported up to 50% longer than their average circumference (Abbaschian 1994; Raman 1995). In this case, the behaviour was captured on video tape. Long bridges were observed for several different encapsulant liquids in separate experiments. An oxide or contaminant layer seemed unlikely in this case. Instead, the thermocapillary effect was recognized as the most likely cause (Saghir, Abbaschian & Raman 1996). We argue that these observations can indeed be qualitatively explained
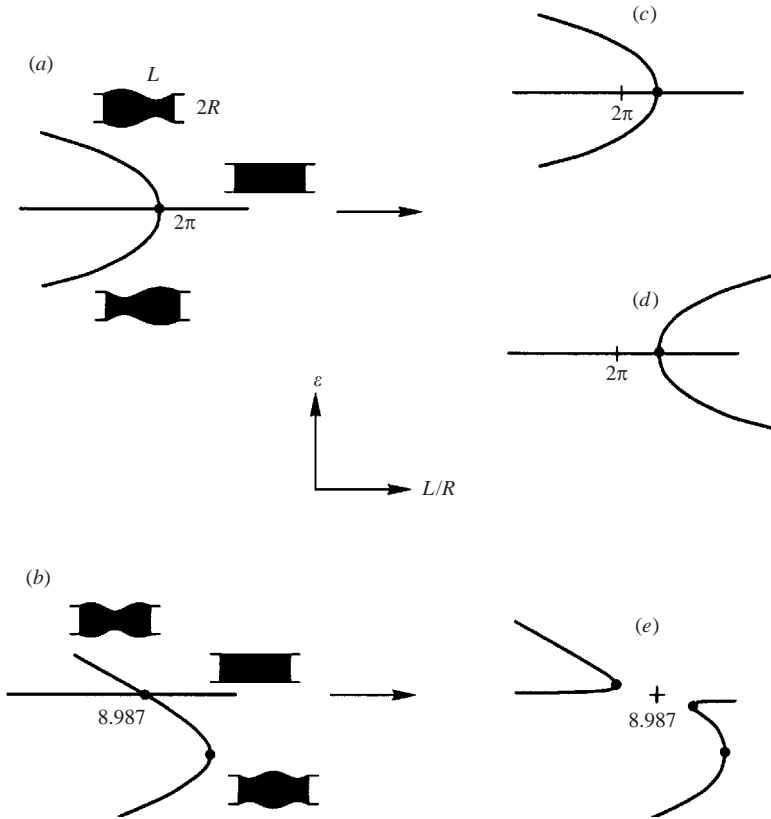
FIGURE 1. Schematic bifurcation diagrams near the first and second interfacial instabilities of a liquid cylinder, showing the branching structures in the ($Ca = 0$) no-flow (a, b) and ($Ca > 0$) flow ($c–e$) cases. The bifurcations (a) and (b) are deformed to (c, d) and (e), respectively, due to the thermocapillary flow induced by a symmetric heating. Solid circles represent singular points. The free-surface shapes of the corresponding branches are sketched in (a) and (b).

by thermocapillary flows. In particular, a competition between capillary and flow-induced pressures can lead to anomalously long stable bridges. The experiments were technically complicated and their primary goal was unrelated to zone length so that details are limited. We present here a simplified model for the interaction. Its predictions are consistent with the limited information from observation.

In zero gravity in the absence of liquid motion, a liquid cylinder of radius R_o becomes unstable at a critical length $L = 2\pi R_o$ (Plateau 1873; Rayleigh 1879), at which length there is a cross-over in dominance of capillary pressures associated with the two principal curvatures of the free surface. The shapes of the static interfaces are governed by the Young–Laplace equation with a volume constraint. These results are now summarized. On increasing its length, a pinned liquid cylinder exhibits a countably infinite sequence of shape instabilities. The shapes correspond to eigenmodes and occur at eigenvalues in a bifurcation analysis. The instability at the Plateau–Rayleigh limit is the first such eigenmode and it has an antisymmetric shape. Destabilizing shapes that are antisymmetric about the bridge midplane alternate with those that are symmetric. In a diagram that plots surface shape deflection against the bridge length (figure 1a, b), the bifurcation diagram, the former class of solutions are pitchfork bifurcations whereas the latter are transcritical bifurcations.

In the presence of liquid motion, an additional pressure gradient contributes to the stress-balance equation and the bifurcation diagram is modified. Symmetry plays a key role in the flow–shape interaction. Flow induced by thermocapillary stress acting symmetrically about the midplane delays the pitchfork bifurcation (figure 1*c*) and breaks the transcritical bifurcations into turning-point singularities (figure 1*e*). Increasing the flow strength further can turn the subcritical pitchfork bifurcation to supercritical, leading to stabilized interfaces (figure 1*d*). In this situation the stability limit jumps to the position of the turning point, and the maximum bridge length can be significantly longer than the classical '2π' limit (figure 1*e*).

It is known that infinite cylindrical interfaces can be stabilized by appropriate axial flow profiles. Xu & Davis (1985) showed that capillary breakup could be suppressed (using isothermal flow) and suggested that long coherent jets could be achieved thereby. The flow convects disturbances along the free surface as travelling waves which can interfere with the destabilizing capillary pressure (Russo & Steen 1989; Hu, Lundgren & Joseph 1990). Stabilizing flow profiles can also be generated by thermocapillarity for annular films (Dijkstra & Steen 1991). The thinness of the annular liquid layer can be used to amplify the stabilizing pressure distribution. Stability analyses of the unbounded cylinder usually use a normal-mode 'temporal' analysis with the perfect cylinder as the base-state solution. In contrast, for bridges of finite length, the translational symmetry along the bridge axis is broken. Consequently, stability analyses are complicated by the closed ends which result in a base state with cellular flow patterns and deformed interfacial shapes that usually cannot be written in analytical form.

A number of studies have incorporated realistic boundary conditions at finite bridge ends in order to examine the dynamics of liquid bridges subject to forced oscillations (Borkar & Tsamopoulos 1991; Mancebo, Nicolas & Vega 1998). All of these studies exclude bridges of lengths close to the PR limit, however. The dynamics they examine does not include competition with the PR capillary instability.

Previous works that look at the interaction of the Plateau-Rayleigh instability with thermocapillary-induced liquid motion are mostly numerical in nature. A challenge of such an approach is capturing the unstable states which emanate as branches at the PR instability. The codimension-two PR singularity has a multiplicity of associated solutions that can be difficult to resolve computationally (Chen, Shen & Lee 1990). Rybicki & Floryan (1987*a*, *b*) report on cellular flow structures and interfacial profiles due to thermocapillary forcing for lengths just short of the PR limit. Chen *et al.* (1990) show that the maximum stable bridge lengths can be changed slightly due to the flow. Dijkstra (1993) considers linear stability of a finite bridge computationally and also reports a small change in maximum stable bridge length for certain flows beneath the interface. In these studies, none of the shifts to longer lengths reported exceeds a few percent.

Mashayek & Ashgriz (1995) study the nonlinear competition between capillary and thermocapillary breakup for periodic disturbances to an infinite cylindrical interface, using finite-element simulation. They solve both the hydrodynamic and thermal problems for a series of initial conditions. They locate the boundary between domains of attraction in part of the parameter space (Reynolds, Marangoni, Biot and capillary numbers). On one side of the boundary, the disturbance evolves to breakup driven by capillary instability, while, on the other side (for the same wavenumber and amplitude), the disturbance evolves to breakup driven by the thermocapillary effect. The boundary is interpreted as a locus where thermocapillary and capillary forces cancel one another – a 'neutral' stability is attained there. In contrast, in the

present paper, conditions are sought to make a previously unstable state stable. Here, 'stabilization' means that disturbances will decay to the stabilized state.

Saghir *et al.* (1996) pose a model that consists of an axisymmetric liquid bridge encapsulated by an outer liquid. They fix the bridge length (about 10% less than the PR limit) and, using the finite-element approach, examine the interface deformation that arises due to the competition between flow-induced pressure of thermocapillary origin and capillary pressure variation along the interface. The choice of encapsulant liquid is varied in an attempt to minimize interface deformation for fixed temperature difference across the ends. They find that the encapsulant with smallest gradient in interfacial tension corresponds to the smallest deformation.

Another group of finite-bridge studies considers an isothermal flow generated by an imposed shear stress at the interface interacting with the PR instability ('half-zone' geometry). That is, the imposed shear is unidirectional. In contrast, the full-zone geometry studied in this paper has zero shear at the midplane by symmetry. Using an approach similar to that of this paper it is found that the nonlinear interaction of the flow and capillary PR instability can combine to yield bridges slightly longer than cylindrical bridges at the PR limit (Chen *et al.* 1999). Experiments are consistent with the predictions (Robinson 2001). In a related study (Atreya & Steen 2002), motivated by experiments that use real-time feed-back control to stabilize the PR mode up to nearly 40% beyond where it is unstable for the uncontrolled system (Robinson 2001), the nonlinear interaction of the flow with the next capillary instability (at $8.9/2\,\pi$ times the PR length) has been analysed and found consistent with experiment.

In the spacelab crystal-growth experiments (STS-57 1993) it was learned that a thin layer of a second fluid surrounding the molten zone (an encapsulent) can improve the interfacial stability (Abbaschian 1994). Interactions among momentum, heat and mass transfer, and phase change during crystal growth makes simulation of the complete physical process cumbersome. In addition, errors in measuring the bridge lengths, owing to instrumentation and a protocol designed primarily for other purposes, limits the information content of the observations. Both these circumstances favour an approach that captures the heart of the mechanism while being insensitive to details of the experiment (or, at least, an approach which recognizes which details do not matter). Bifurcation analysis couched in singularity theory is precisely such an approach. Its power in similar situations has been demonstrated in numerous instability phenomena in fluid and solid mechanics (Stewart 1981), including the Ruelle–Takens scenario for the transition from laminar to turbulent flow (Guckenheimer 1986).

In this paper, we present a model problem for the influence of flow on the Plateau–Rayleigh instability. The aim is to capture without unnecessary detail the relevant physics that accounts for interfacial stabilization under the action of the thermocapillary flows. For simplicity, we shall assume a liquid bridge of fixed length and non-isothermal free surface, and ignore the melting and solidification processes. To illustrate the stabilization mechanism, we model the bridge as a thin layer of liquid (the molten metal) with an interface that is subjected to a stress of thermocapillary origin. The bridge liquid surrounds a solid core. The extent of the solid core is a control parameter in the model. The effect of the thin external encapsulant layer is felt through the interfacial stress balance. Fluid motion in the encapsulant is not explicitly modelled. According to the model, the flow-induced lubrication pressure competes with the capillary tension and helps to stabilize the free surface. The formulation is set up as a bifurcation problem. The symmetry issues involved are discussed in the context of the underlying bifurcation structures (the universal unfolding). Singularity theory and normal-form analysis are employed. They are well-suited to revealing the
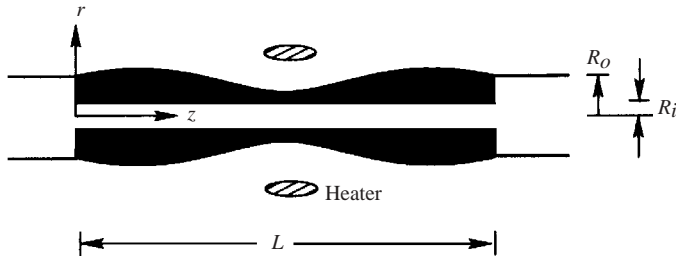
FIGURE 2. Liquid float zone in zero gravity, with an outer radius R_o, a solid core R_i, and a ring-like heater placed at the midsection of the bridge.

richness of the nonlinear interaction and to identifying which 'imperfections' are the most sensitive near instability. We then discuss what could be expected in the crystal-growth experiments where a second layer of liquid is employed (the encapsulant).

We organize the remaining sections as follows. In §2 we set down the basic assumptions that lead to the flow-modified Young–Laplace problem. Symmetric heating, simulating a full floating zone, induces the thermocapillary stress. The lubrication approximation is used to model the flow-induced pressure. Bifurcation analyses including numerical branch-tracing calculations and a Lyapunov–Schmidt reduction are presented in §3; bifurcation diagrams show the effects of the flow upon various eigenmodes of the capillary instability. The main result is the suppression of the Plateau–Rayleigh limit. The birth of limit cycles corresponding to standing waves is also predicted. A brief discussion in §4 closes our presentation.

2. Interfacial balance equation

Consider a long axisymmetric cylindrical liquid annulus with an inner radius R_i and outer radius R_o encircled by a ring-like heater (figure 2). The 'free' outer (fluid–liquid) and the inner (liquid–solid) interfaces bound a layer of Newtonian liquid, forming a liquid bridge in zero gravity. The heater creates a temperature difference ΔT along the free surface, which results in a surface-tension variation $\Delta\sigma$ below a reference value $\bar{\sigma}$. The liquid density ρ and viscosity μ are assumed to be constants, independent of temperature. A passive gas of negligible density and viscosity surrounds the free surface. The thermocapillary stress induces a motion in the liquid.

We examine the situation when the viscous force of the liquid balances the thermocapillary force. The velocity, length, pressure and temperature scales refer to $V \equiv \Delta\sigma/\mu$, R_o, $\mu V/R_o$ and ΔT, respectively. A cylindrical coordinate system (z, r) is employed, where the z-axis coincides with the bridge centreline and u is the velocity component in the z-direction. An aspect ratio $A \equiv 1 - R_i/R_o$ represents the average thickness of the liquid layer, $l \equiv L/R_o$ denotes the bridge length, and $\hat{\sigma} \equiv \sigma/\bar{\sigma}$ is the scaled surface tension.

We assume surface tension to be a linear function of surface temperature, $\hat{\sigma} = 1 - Ca\,T$, where the capillary number Ca is defined as

$$Ca \equiv -\frac{\partial_T \sigma \, \Delta T}{\bar{\sigma}} \geqslant 0, \tag{2.1}$$

measuring the strength of the thermocapillary effect. In principle, the interfacial temperature can be obtained by solving the heat equation and appropriate boundary conditions. Here, we use a sinusoidal function, $T = \sin(\pi z/l)$, $z \in [0, l]$, to model

the temperature distribution. This distribution simulates the effect of external heating that is symmetric about the midplane of the liquid column and may be realized in the limit of large heat-transfer coefficients (large Biot numbers), in which case the temperature of the free surface approximately equals the temperature in the ambient. The sinusoidal profile is viewed as the leading-order approximation in a Fourier expansion of the ambient temperature. The surface tension is then given by

$$\hat{\sigma} = 1 - Ca \sin(\pi z/l), \tag{2.2}$$

and the momentum transport is coupled with the heat transport only through this imposed condition. The liquid motion is driven by a prescribed shear stress acting upon the free surface.

According to (2.1), the case $Ca = 0$ occurs when the bridge is isothermal or in the limit of large reference surface tension. The latter limit is not of interest, as reflected in the chosen scaling (for $Ca = 0$, the scaled $\hat{\sigma} = 1$ rather than 0), since then the interface is non-deformable. The present stabilization mechanism requires capillary deformation.

For thin liquid layers and slow fluid motions a lubrication approximation is appropriate to describe the flow profile induced by the thermocapillary stress. The velocity u is obtained by integrating the Stokes equation

$$r^{-1}\partial_r(r\,\partial_r u) = \partial_z p, \tag{2.3}$$

which yields a type of core–annular flow relating velocity u, pressure gradient $\partial_z p$, and shear stress τ_s on the free surface:

$$u(z, r, t) = \tfrac{1}{2}h \ln(r^2/\omega^2)\,\tau_s - \tfrac{1}{4}[\omega^2 - r^2 + h^2 \ln(r^2/\omega^2)]\,\partial_z p. \tag{2.4}$$

Here, $r = h(z, t)$ defines the shape of the free surface, and $\omega \equiv R_i/R_o = 1 - A$ denotes the relative position of the inner radius where the motion must vanish. The momentum transport in the radial direction has been neglected and hence $p = p(z, t)$. This is justified by the thinness of the liquid layers resulting from the long-bridge (or small-aspect-ratio) configuration ($A/l \ll 1$). The appropriate measure of inertia to viscous force in the bridge liquid is $A/l(\rho V R_0/\mu)$ (a Reynolds number). Note that, although we refer to the flow model as the 'lubrication approximation', this assumption is consistent with a 'rectilinear flow' approximation (common in coating flow analyses) which can be appropriate for Reynolds numbers of order one and greater for thin layers provided deformations are small and turning regions occupy a small fraction of the flow domain.

We shall also assume that the fluid, liquid and solid phases meet at sharp corners, such that the free surface is pinned at the two ends of the bridge: $h = 1$ at $z = 0$ and $z = l$. The interfacial shape is axisymmetric, encloses a cylindrical volume

$$\int_0^l h^2 \, \mathrm{d}z = l, \tag{2.5}$$

and satisfies the mass-conservation equation

$$\partial_t h^2 + \partial_z \int_\omega^h 2u \, r \mathrm{d}r = 0. \tag{2.6}$$

The turning flow patterns near the two bridge ends are neglected, but the finite-end effect is accounted for by the zero-flux condition through each cross-section:

$$\int_{\omega}^{1} u \, r \mathrm{d}r = 0 \quad \text{at} \quad z = 0 \quad \text{and} \quad z = l. \tag{2.7}$$

In this lubrication approximation, the normal stress and tangential stress balances at the free surface are governed by the equations

$$p = Ca^{-1}\hat{\sigma} K(h), \quad \tau_s = Ca^{-1}\partial_z\hat{\sigma}, \tag{2.8}$$

where $K(h)$ is the curvature:

$$K(h) \equiv \frac{1}{h[1 + (\partial_z h)^2]^{1/2}} - \frac{\partial_z^2 h}{[1 + (\partial_z h)^2]^{3/2}}. \tag{2.9}$$

Combining the flow field (2.4) with the mass conservation (2.6), integrating twice and applying stress balance equations (2.8), one obtains

$$\int_0^z \left[\frac{\varXi(h)}{\Theta(h)} \partial_z\hat{\sigma} + \frac{Ca}{\Theta(h)} \int_0^z \partial_t h^2 \mathrm{d}z' \right] \mathrm{d}z + P_s = \hat{\sigma} K(h), \tag{2.10}$$

in which $\varXi$ and Θ are functionals of the interfacial shape,

$$\varXi(h) \equiv h \int_{\omega}^{h} \ln(r^2/\omega^2) \, r \mathrm{d}r, \tag{2.11}$$

$$\Theta(h) \equiv \tfrac{1}{2} \int_{\omega}^{h} [\omega^2 - r^2 + h^2 \ln(r^2/\omega^2)] \, r \mathrm{d}r. \tag{2.12}$$

Equation (2.10) describes the evolution of the free surface with pinned boundaries. The functionals $\varXi$ and Θ result from the integration, and the static pressure P_s and zero-flux condition (2.7) supply the integration constants. The integral term in (2.10) expresses the flow-induced pressure. Let $H \equiv h - \omega = h + A - 1$ denote the liquid film thickness. It can be readily shown that

$$u = O(A/l), \quad \varXi \sim H^2, \quad \Theta \sim \tfrac{2}{3}H^3, \quad K \sim 1 - H - \partial_z^2 H, \tag{2.13}$$

when $A \ll 1$. Equation (2.10) then becomes a 'Hammond'-type long-wave equation for the dynamics of thin liquid films, but written in integral form and coupled with thermocapillary convection (Hammond 1983; see also Oron, Davis & Bankoff 1997 for a review). We shall retain here the form of a core–annular flow to include the case of completely molten cores in long bridges ($A \sim 1$, $l \gg 1$). In the balance equation, the capillary pressure due to the shape curvatures is exact but the flow-induced pressure is an approximation. This approach has been applied to model breakup of viscous jets (Eggers & Dupont 1994) and capillary films (Gauglitz & Radke 1988) and has been shown to give satisfactory results even when the free surfaces have large deformations.

3. Bifurcation structures

Equation (2.10) can be thought of as a bifurcation problem in length l with cylindrical interface ($h \equiv 1$) and quiescent liquid as the base state. In the absence of flow ($Ca \equiv 0$) the Young–Laplace problem is recovered in which the static pressure P_s corresponds to the Lagrange multiplier of the volume constraint in an appropriate

energy minimization formulation (Gillete & Dyson 1971). The presence of the flow introduces an unfolding parameter Ca which perturbs the solutions away from the base-state solution. For convenience in the bifurcation analysis, we stretch the coordinate using a new variable $x \equiv z/l$. Thus, the interface deflection function, defined as

$$\eta(x) \equiv h^2 - 1,$$

has fixed boundary and volume constraints independent of the bridge length l: $\eta(0) = \eta(1) = \int_0^1 \eta(x)\mathrm{d}x = 0$. We then treat l as the preferred bifurcation parameter. The steady-state problem is defined through a mapping,

$$F(h;l,Ca) \equiv \hat{\sigma}(x;Ca)\,K(h;l) - P_s - \int_0^x \frac{\varXi(h)}{\Theta(h)}\,\partial_x\hat{\sigma}(x;Ca)\,\mathrm{d}x, \qquad (3.1)$$

where solutions of (2.10) correspond to the null space of this mapping. Note that $\partial_z = l^{-1}\partial_x$ so that the curvature K is a function of l after the transformation. The static pressure scalar P_s is viewed as a bounded functional acting on the solution space. Aspect ratio A is suppressed in the notation of (3.1).

Let $\mathrm{D}_\eta F$ define the Frechet derivative of the map F with respect to η. Solving the linear problem,

$$\mathrm{D}_\eta F(1;l,0)\eta = -\tfrac{1}{2}\big(\eta + l^{-2}\partial_x^2\eta\big) - P_s + 1 = 0, \qquad (3.2)$$

one finds two categories of non-trivial solutions:

(AS) antisymmetric modes: $(\eta, l) = (\phi_n, \ell_n)$,

$$\phi_n = \sin(\ell_n x), \quad \ell_n = 2n\pi, \qquad (3.3)$$

(CS) centro-symmetric modes: $(\eta, l) = (\varphi_n, \mathfrak{L}_n)$,

$$\varphi_n = 2\mathfrak{L}_n^{-1}\big[\cos(\mathfrak{L}_n x) + \tfrac{1}{2}\mathfrak{L}_n \sin(\mathfrak{L}_n x) - 1\big], \quad \tan(\mathfrak{L}_n/2) = \mathfrak{L}_n/2, \qquad (3.4)$$

where n are positive integers. Type-(AS) solutions deform antisymetrically about the midplane of the bridge. The solutions have a flip symmetry: $\phi_n(x) = -\phi_n(1-x)$, and the first eigenmode bifurcates at $\ell_1 = 2\pi$, corresponding to the classical Plateau–Rayleigh limit (cf. figure 1a). Type-(CS) possesses a reflection symmetry: $\varphi_n(x) = \varphi_n(1-x)$, in which the interfaces deform centro-symmetrically and the first bifurcation point occurs at $\mathfrak{L}_1 \approx 8.987$ (cf. figure 1b). The (AS) solutions are related to sinusoidal normal-mode perturbations in the analysis of infinitely long bridges, whereas the (CS) solutions arise due to the finite-bridge geometry. The ℓ_1- and $\mathfrak{L}_1$-mode are the most dangerous among each of the two classes of solutions as bridge length increases. Their interaction with the fluid motion is the focus of the following analysis.

3.1. *Branch-tracing calculation*

The flow-induced pressure and nonlinearity in the curvature modify solutions from the linear state. Equation (3.1) defines a two-point boundary value problem with an integral constraint. In figure 3, typical bifurcation diagrams obtained using the numerical branch-tracing method (Doedel 1981) illustrate how the first two modes, ℓ_1 and $\mathfrak{L}_1$, are affected by the flow and by each other through the flow. The starting point is a cylindrical state ($\eta = 0$) in the no-flow condition, with length l and aspect ratio A fixed. The numerical calculation traces the solutions in the parameter space (l, Ca, P_s, A). Two state variables are defined using projection on the function space
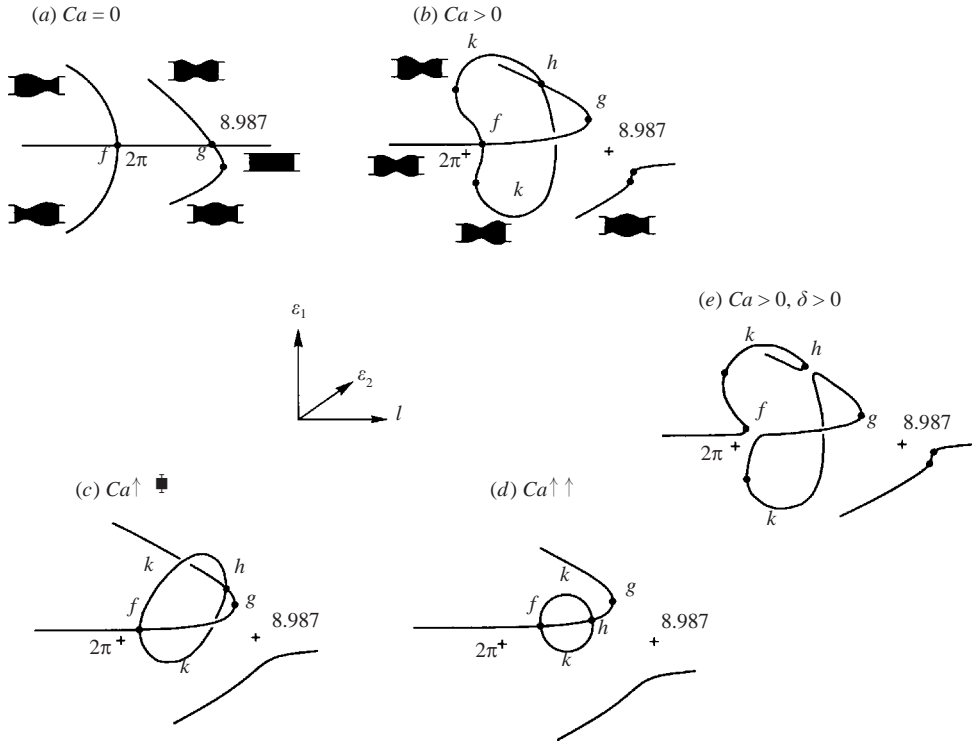
FIGURE 3. Schematic bifurcation diagrams obtained from numerical branch-tracing calculations. The strength of the thermocapillary force increases from (*a*) to (*d*). The parameter δ breaks the midplane symmetry in (*e*). Solid circles represent singular points. The free-surface shapes of the corresponding branches are sketched in (*a*) and (*b*).

to measure the amplitudes of the solutions:

$$\tfrac{1}{2}\varepsilon_1 = \langle \eta, \phi_1 \rangle = \int_0^1 \eta\,\phi_1\mathrm{d}x, \qquad (3.5)$$

$$\tfrac{1}{2}\varepsilon_2 = \langle \eta, \varphi_1 \rangle = \int_0^1 \eta\,\varphi_1\mathrm{d}x. \qquad (3.6)$$

The bifurcation structures near the singular points in the quiescent case ($Ca \equiv 0$) are predicted by the symmetry issues alluded to above (§1). Nonlinearity in the curvatures produces a subcritical pitchfork and a transcritical bifurcation, lying on the (l, ε_1)- and (l, ε_2)-planes, respectively (figure 3*a*; see also figure 1*a*, *b*). They correspond to the pure-mode solutions. The effect of the thermocapillary flow ($Ca > 0$, figure 3*b*) is (i) to deform those branches by shifting the pitchfork bifurcation point away from the classical 2π limit, and (ii) to break the transcritical singularity into a pair of turning points. Numerical data indicate that the flow promotes $\mathfrak{L}_1$ instability ($l < 8.987$) but delays the ℓ_1-mode bifurcation ($l > 2\pi$) by an amount proportional to the magnitude of Ca. Thus, bridges can be stable even when the lengths are longer than the Plateau–Rayleigh limit. Among those solutions, shape deformations following the $\overline{fgh}$ branch contain only the $\mathfrak{L}_1$-mode. The bifurcation curves lie entirely within the (l, ε_2)-plane. In contrast, branches following $\overline{fkh}$ contain mixed modes and form a loop in the ($l, \varepsilon_1, \varepsilon_2$)-space. By further increasing the value of Ca it is possible to 'turn over'
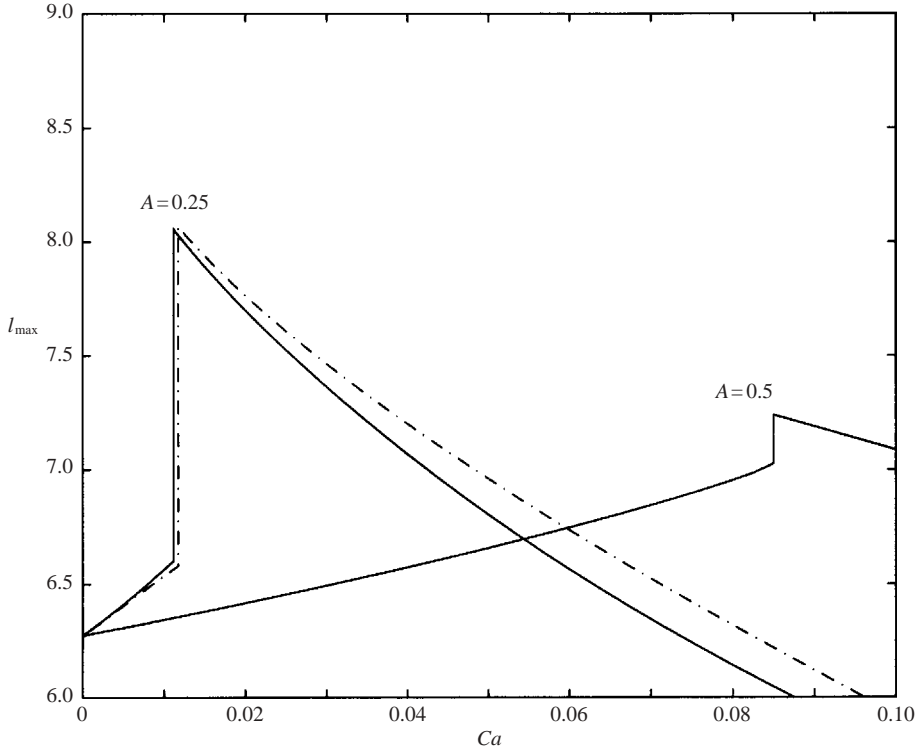
FIGURE 4. Maximum stable bridge length l_{max} versus the capillary number Ca for $A = 0.25$ and $A = 0.5$. Dashed-dotted line represents results from the Lyapunov–Schmidt reduction procedure (§3.2).

the pitchfork to a supercritical bifurcation (figure 3c, d; see also figure 1d), so that mixed-mode solutions $\overline{fkh}$ are stabilized and the stable lengths are extended to the turning-point g in the diagram. In summary, the flow-induced pressure deforms the original unstable branches and results in stabilization.

Figure 4 plots the maximum bridge length l_{max} as a function of the thermocapillary strength Ca, for different aspect ratios A. The region above the marginal stability curve is unstable. The solid curves from continuation computations are loci of the relevant singular point (f or g) with increasing values of Ca and are compared with the dash-dot line from the Lyapunov–Schmidt method (§3.2). It is seen that the marginal stability boundary has a jump at Ca^*. There, the subcritical pitchfork bifurcation turns supercritical (figure 3c) and the length l_{max} suddenly jumps from the value at the first bifurcation (f) to that at the second bifurcation point (g). Beyond Ca^*, the classical Plateau–Rayleigh instability is shielded by the fluid motion. Figure 4 also indicates that this critical stress Ca^* occurs earlier for a thinner liquid annulus (small A), suggesting that the lubrication flow in a thin film will greatly enhance the stability with l_{max} approaching $\mathfrak{L}_1 \approx 8.987$ in the extreme case.

Regarding the numerical calculation, we remark that it is difficult to perform branch continuation directly on a pitchfork singularity since the pitchfork is not structurally stable. Nevertheless, a turning point is robust (codimension 0) and its continuation produces reliable results. Thus the loci of turning point g can be found in a straightforward manner ($Ca > Ca^*$) to produce the maximum bridge length.

In contrast, when tracing the pitchfork bifurcation f in the range of $Ca < Ca^*$, the formulation (3.1) is modified as follows. Before branch continuation starts, the pitchfork at f is broken into turning points (figure 3e) by introducing an artificial perturbation δ in the static pressure: $P_s \mapsto P_s + \delta x$, where $\delta = 10^{-6}$ is used. A non-zero δ is equivalent to a residual acceleration in the axial direction of the bridge, which breaks the midplane symmetry of the heating. The pitchfork is then viewed as the limit of the turning points as $\delta \to 0$. In producing figure 4 we start at a point on the trivial branch, $(\eta, Ca) = (0, 0)$, with a given length $l < 2\pi$. The solution is then traced using (δ, P_s) as free parameters. When the branch reaches $\delta = 10^{-6}$ we change the free parameters to (l, P_s) and follow the branch until the turning point is found (figure 3e). Its position should approximate that of the pitchfork bifurcation. At this point, the system is lifted by appending $F = 0$ with an additional condition that demands $D_\eta F$ to be singular, and the continuation is performed in the (l, Ca, P_s) parameter space. Parameter δ, acting as a gravity imperfection on the symmetry (Chen *et al.* 1999), introduces a shift $\Delta l = O(\delta^{2/3})$ in the true position of the pitchfork bifurcation. To test the modified approach, exact branching positions for $\delta \equiv 0$ are explicitly calculated for several Ca values without using the continuation technique; they are indistinguishable from the results shown in the figure found by the modified approach.

3.2. *Symmetry issues and universal unfolding*

Near the singular points the bifurcation structures can be obtained analytically by the Lyapunov–Schmidt reduction procedure (Golubitsky & Schaeffer 1985). For the (AS)-type solutions, we rescale the bridge length and shape deformation function as

$$\lambda_1 = 1 - (2\pi/l)^2, \quad \eta(x) = \varepsilon_1\phi_1(x) + w_1(x), \tag{3.7}$$

where w_1 is set to be orthogonal to ϕ_1: $\langle w_1, \phi_1 \rangle = 0$. The nonlinear map $F(h; l, Ca)$ is reformulated as $\widetilde{F}(\eta; \lambda_1, Ca)$ so that the singular point of F is shifted to the origin $(\eta, \lambda_1, Ca) = \mathbf{0}$. The projection of F (dropping the tilde) onto the null space ϕ_1,

$$g_1(\varepsilon_1; \lambda_1, Ca) = \langle F(\varepsilon_1\phi_1 + w_1; \lambda_1, Ca), \phi_1 \rangle, \tag{3.8}$$

provides the local structure of the bifurcation, in view of the self-adjointness of the linear problem (3.2). The graph of $g_1 = 0$ then gives the bifurcation curves near the singularity. The perturbation function $w_1(x)$ can be shown to be $o(\varepsilon_1)$ and is obtained by solving the complementary equation, $F - g_1\phi_1 = 0$, where the singularity has been factored out.

The bifurcation equation for the second singularity, $g_2 = 0$, can be obtained by the same procedure. The corresponding transformations for the bridge length, shape function and projected map are

$$\lambda_2 = 1 - (\mathfrak{L}_1/l)^2, \quad \eta(x) = \varepsilon_2\varphi_1(x) + w_2(x), \tag{3.9}$$

$$g_2(\varepsilon_2; \lambda_2, Ca) = \langle F(\varepsilon_2\varphi_1 + w_2; \lambda_2, Ca), \varphi_1 \rangle. \tag{3.10}$$

Note that in this case the singular point of the basic state is at $(\eta, \lambda_2, Ca) = \mathbf{0}$.

In the formulation, the long-bridge/small-aspect-ratio condition justifies the lubrication-type flow assumption which provides the coupling to the interface shape. The flow-induced pressure therefore depends on the given flow model. Nevertheless, certain characteristics of the balance equation can be inferred on physical grounds and are independent of the specific model. It is therefore instructive to first examine a few generic properties of the 'reduced' functions (g_1, g_2) before presenting the model-dependent results. Those properties are reflected in the structures of the reduced

bifurcation functions. Two observations are in order. (i) Owing to heating at the mid-position, any nonlinear map F which portrays the stress balance on the free surface must possess a reflection symmetry

$$F(\gamma \eta; \lambda_1, Ca) = \gamma F(\eta; \lambda_1, Ca), \tag{3.11}$$

where $\gamma: u(x) \to u(1-x)$. The equivariance property (3.11) forces the consequent g_1 to also preserve the symmetry:

$$g_1(-\varepsilon_1; \lambda_1, Ca) = -g_1(\varepsilon_1; \lambda_1, Ca). \tag{3.12}$$

Generically, (3.12) corresponds to a pitchfork structure (cf. figure 3*a*). (ii) The symmetry of the thermocapillary stress demands $\langle \mathrm{d}F(0; \lambda_2, 0)/\mathrm{d}Ca, \varphi_1 \rangle \neq 0$. By the implicit function theorem (Iooss & Joseph 1981) we infer that there exists a unique branch of solutions $Ca = \widehat{Ca}(\varepsilon_2, \lambda_2)$ near $(\varepsilon_2, \lambda_2) = 0$. Applying the above inequality to the definition of g_2 gives the condition

$$\frac{\mathrm{d}g_2(0; 0, 0)}{\mathrm{d}Ca} \neq 0, \tag{3.13}$$

which implies that, in the presence of the flow, the transcritical breaks into a turning-point bifurcation (cf. figure 3*b*).

The structure of the bifurcation functions for the lubrication model will now be given. It can be checked that the conditions just discussed for the general case hold for the specific model. By the procedures outlined, the reduced map $\boldsymbol{g} \equiv (g_1, g_2)$ represents a projection of the nonlinear function onto (ϕ_1, φ_1) near each of the bifurcation points. The result, written as expansions of ε_i, is found to be

$$g_1 \sim \left(-\tfrac{3}{32} + \xi_3 Ca\right) \varepsilon_1^3 + \left(-\tfrac{1}{4}\lambda_1 + \xi_1 Ca\right) \varepsilon_1 = 0, \tag{3.14}$$

$$g_2 \sim -\frac{1}{2\mathcal{L}_1}\varepsilon_2^2 - \tfrac{1}{4}\lambda_2\varepsilon_2 - \xi_0 Ca = 0. \tag{3.15}$$

In these equations, the coefficients

$$\xi_0 \sim \frac{6\mathcal{L}_1}{\pi A\left(\mathcal{L}_1^2 - \pi^2\right)} \left(1 - \frac{A}{3} + \frac{A^2}{10}\right), \tag{3.16}$$

$$\xi_1 \sim \frac{2}{5\pi A^2}\left(1 + \frac{7A}{30} + \frac{3A^3}{20}\right), \quad \xi_3 \sim \frac{8}{105\pi A^4}\left(1 + A + \frac{157A^2}{256}\right), \tag{3.17}$$

are obtained through the reduction procedure and expressed in the small-A limit. The coefficient ξ_0 is given by directly evaluating the integral in the formula,

$$\xi_0 Ca = \left.\frac{\varXi}{\varTheta}\right|_{h=1} \langle \hat{\sigma}(x; Ca), \varphi_1 \rangle. \tag{3.18}$$

To obtain ξ_1 and ξ_3 one must solve for the shape deflection functions $w_i(x)$ at each order. The unfolding parameter Ca preserves the pitchfork but breaks the transcritical bifurcations present in the classical Young–Laplace problem. A thin-film configuration (small A) further amplifies this perturbation through the coefficients ξ_i.

The amplitude of the surface shape is obtained from $\boldsymbol{g} = \boldsymbol{0}$ (3.14), (3.15). The thermocapillary flow induces a deformation

$$\varepsilon_1 = 0, \quad \varepsilon_2 = -\tfrac{1}{4}\mathcal{L}_1\lambda_2\left[1 - \left(1 - \frac{32\xi_0}{\mathcal{L}_1\lambda_2}Ca\right)^{1/2}\right], \tag{3.19}$$

which recovers the cylindrical state, $\varepsilon_1 = \varepsilon_2 = 0$, when $Ca = 0$. A straightforward calculation using (3.14), (3.15) also gives the positions of the two bifurcations (the pitchfork f and turning point g) and the criteria Ca^* at which the pitchfork solutions turn supercritical. Those singular points are located by the formula $g_i = \mathrm{d}g_i/\mathrm{d}\varepsilon_i = 0$, and the maximum stable bridge length is given by

$$l_{\max} \sim \begin{cases} 2\pi(1 + 2\xi_1 Ca), & 0 < Ca < Ca^*, \\ \mathfrak{L}_1\left[1 - (8\xi_0 Ca/\mathfrak{L}_1)^{1/2}\right], & Ca^* < Ca \ll 1. \end{cases} \tag{3.20}$$

Here, $Ca^* \sim 3/(32\xi_3)$ is derived by setting the coefficient of the cubic term in g_1 to zero. Figure 4 plots the estimate of maximum bridge length using this formula for $A = 0.25$ (dash-dot line). This compares favourably with the results of the branch-tracing calculation. Equations (3.14), (3.15) exhibit properties (i, ii) discussed above and so provide a specific example of generic features near the two bifurcations. For Ca^* predicted by the Lyapunov–Schmidt expansion to remain faithful to the branch-tracing results when A is not small, more terms will be required in the coefficient of the cubic term.

4. Discussion

The bifurcation diagrams obtained alternatively by computation and by analysis may be summarized from a broader viewpoint, one that views the two-mode interaction as a local interaction. The system falls into a class of bifurcation problems in two state variables with $\mathbf{Z}_2$ invariance: $(r, s) \mapsto (-r, s)$. By appropriate transformations of variables the reduced functions (3.14), (3.15) can be put into a normal form with the same symmetry:

$$\boldsymbol{g} = [(ms^2 - \beta s + r^2 - \alpha)r, s^2 + r^2 - \lambda], \tag{4.1}$$

$$s \sim \frac{-\lambda_2}{8}(2\mathfrak{L}_1)^{1/2} - \frac{\varepsilon_2}{(2\mathfrak{L}_1)^{1/2}}, \quad r \sim \varepsilon_1, \quad \lambda \sim \frac{\mathfrak{L}_1}{32}\lambda_1^2 - \xi_0 Ca, \tag{4.2}$$

where (α, β, m) are unfolding parameters (Golubitsky, Stewart & Schaeffer 1988). Note that (4.1) is suitable for describing the solutions near the double degeneracy $(r, s) = \mathbf{0}$, while (3.14), (3.15) depicts the projection of the nonlinear function F onto each singularity. A mapping between parameters (α, β, m) and (l, Ca, A) can be obtained if the reduction problem is set up and solved at the double-degenerate point. This mapping has not been carried out. Yet, even without the detailed mapping, predictions of (4.1) are useful.

The normal form (4.1) renders the stability and predicts the domains of attraction of the branching solutions within the context of the corresponding two-dimensional system. In view of the absence of inertia and consistent with the lubrication model (2.10), the 'reduced' dynamics has a gradient-flow structure:

$$(\dot{r}, \dot{s}) + \boldsymbol{g}(r, s; \lambda, \alpha, \beta, m) = 0. \tag{4.3}$$

Here, the overdot indicates the time derivative with an appropriate time scale. Its universal unfolding has been solved and all possible bifurcation diagrams are catalogued in Golubitsky *et al.* (1988, p. 144). The bifurcation diagrams produced from (3.14), (3.15) recover some of the diagrams in the catalogue (figure 3). By comparing the branching structures of the two problems (2.10) and (4.3) we infer that the eigenvalues of (r, s) modes should agree with those of $(\varepsilon_1, \varepsilon_2)$ in a linear stability analysis. Figure 5(*a*) illustrates this comparison, in which the signs $+/-$
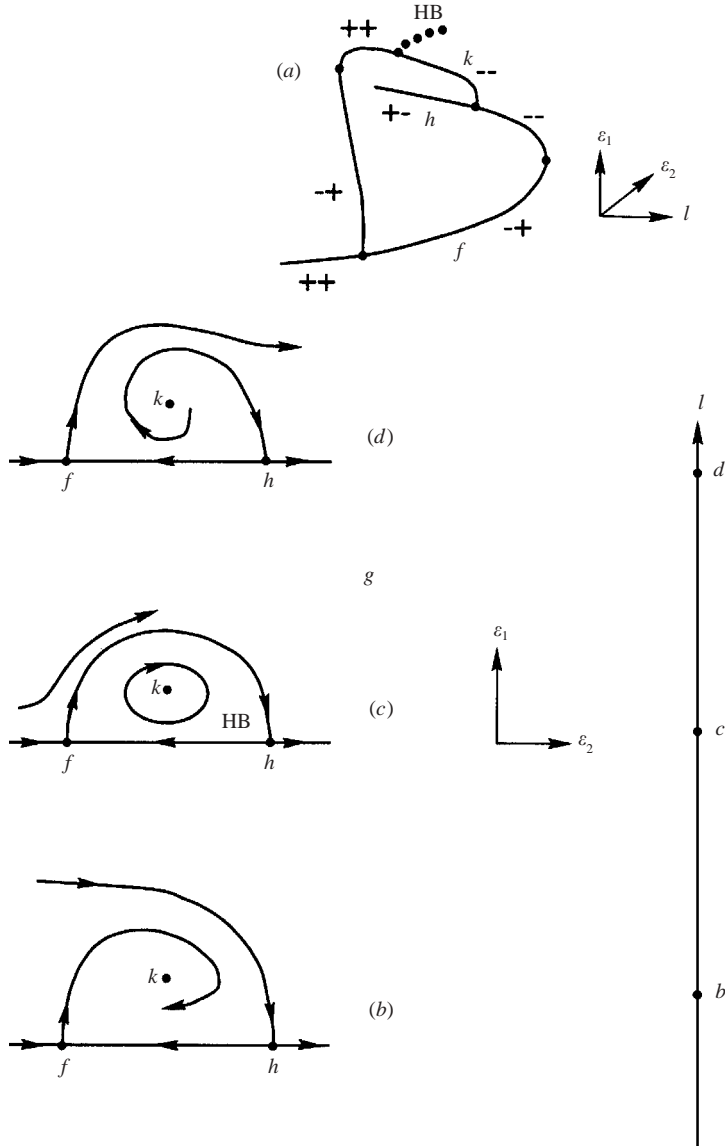
FIGURE 5. Bifurcation of vector fields near the Hopf bifurcation 'HB'. Path followed by increasing the bridge length with a fixed capillary number Ca.

denote stability/instability of the corresponding modes. A prediction of the normal form (4.1) but not of (3.14), (3.15) is the existence of a Hopf bifurcation corresponding to standing-wave patterns in the physical system. The discrepancy arises since the 'local' interactions included in (4.1) are less local than those in (3.14), (3.15). Guided by this prediction, we have directly integrated (2.10) for a few cases. Indeed, the full model shows the birth of a limit cycle in a small window of the parameter space. A homoclinic orbit encloses a time-periodic solution after collision of the two invariant manifolds; figure 5($b-d$) shows a sketch. The cycle grows with an increasing period and amplitude, collides with the homoclinic orbit and disappears suddenly. Properties of such periodic solutions have been examined extensively (Żolądek 1984; Arnol'd

1991). It turns out that detailed mappings between (2.10) and (4.1), (4.3) are needed in order to use those results to understand the current system, however. Here, one should note that the periodic solution arises due to mode–mode interaction among capillary instabilities, whose origin is different from those oscillatory solutions observed in short bridges ($l \approx 1$) of high Reynolds numbers where hydrodynamic instability and non-axisymmetry are important (Kuhlmann & Rath 1993).

The mechanism of stabilization near $l_1 = 2\pi$ is a suppression of the capillary disturbance through modification of the interfacial pressure profile. Referred to the unit interval ($0 \leqslant z \leqslant 1$), the destabilizing capillary mode has a $\sin(2\pi z)$ shape with a corresponding pressure profile that drives fluid from the neck ($z = 3/4$) to the bulge ($z = 1/4$). The thermocapillary flow driven by heating at the midplane ($z = 1/2$) results in a pressure profile driving an axial return flow (away from the interface) that that opposes the capillary flow; the pressure is also antisymmetric about the midplane. The corresponding thermocapillary-induced deflection $-\sin(3\pi z)$ has a neck at the midplane. This is consistent with a planar layer where it is known that a bulge occurs under a hot spot owing to thermocapillary flow. The thermocapillary-induced pressure profile opposes the capillary flow over ($1/4 \leqslant z \leqslant 3/4$) with a net stabilizing effect.

Details of this mechanism are reflected in and can be traced through the bifurcation equation (3.14). For example, modifications to the motionless base state are represented by terms proportional to Ca. According to equation (3.1) this can be a weakening of surface tension under the hot midplane to influence the 'capillary pressure' (first term on the right) or can be the flow-induced 'thermocapillary pressure' (last term on the right). It turns out that the order-ϵ_1 stabilization ($\xi_1 Ca$ term in equation (3.14)) is due solely to the latter influence. Indeed, the thermocapillary pressure has a structure ($\cos(\pi z)$ and $\cos(3\pi z)$) with signs that project on the capillary pressure $\sin(2\pi z)$ in a stabilizing way. In a similar fashion, the order-ϵ_1^3 stabilization can be traced to the thermocapillary flow (the dependence of ξ_3 on A makes this clear). Here, the effect of flow is to weaken the subcritical nature of the capillary instability (geometrically, lessen the curvature of the 'pitchfork' in the pitchfork bifurcation). The surprising result of the finite-amplitude computations is that this stabilizing effect can 'turn the bifurcation over' – can change it from a subcritical to a supercritical bifurcation.

In assessing the relevance of the proposed model, good estimates from spacelab experiments for the strength of the thermocapillary force and the amplitude of the interfacial deformation are most important. Gravity plays a minor role in the microgravity environment, yet any perturbation that introduces a midplane asymmetry is accounted for by an unfolding diagram similar to figure 3(*e*); see §3.1. Bifurcation analysis shows that the critical stress is at $Ca^* \propto A^4$ for small A, at which stress the length l_{max} jumps to the value of the second bifurcation point (ε_2-mode), whose value is close to $\mathfrak{L}_1 \approx 8.987$ and is roughly 50% longer than the classical 2π-limit. A thin layer of liquid reduces the velocity scale ($u = O(A)$) but greatly enhances the magnitude of the lubrication pressure that suppresses the Plateau–Rayleigh instability (cf. equation (3.14)). In practice, employing a thin layer of viscous liquid which encapsulates a bridge can achieve the same purpose. The induced flow in the outer fluid (encapsulant) provides an extra pressure gradient in addition to that in the liquid column. Its effect is to reduce the surface deflection and lower the flow magnitude further (Saghir *et al.* 1996). Under this circumstance, encapsulated bridges should be more stable than bridges of single fluids.

In the spacelab experiments that motivated this study, heating power controlled the length of the melt (liquid bridges). Various encapsulants (liquids and gas) isolated

the bridges from the surroundings. Once the long molten zones were formed, the flow-induced pressures in the inner liquid and outer fluids together acted as an interfacial stabilizing agent, shielding the liquid columns from breaking apart. The lubrication pressure is important whether it arises from the inner (bridge) or outer (encapsulant) liquid. It is proposed here that the symmetrical heating that generates the thermocapillary flows is the key physical feature responsible for the extra-long bridges observed. In the model, the lubrication pressure arises from the inner liquid. The limited observations from the space experiments preclude a rigorous test of this proposal. We do not know the extent of the solid core, if any, for example. The predictions in this paper of extra-long finite bridges are testable, however, and provide a guide for what to look for in future ground-based experiments, should they be undertaken.

REFERENCES

ABBASCHIAN, R. 1994 Liquid encapsulated molten zone (LEMZ) processing on STS-57. *AIAA Paper* 94-0563.

ARNOL'D, V. I. 1991 *Dynamical Systems V: Bifurcation Theory and Catastrophe Theory*. Springer.

ATREYA, S. & STEEN, P. H. 2002 Stability analyses of long liquid bridges in the presence of gravity and flow. *Proc. R. Soc. Lond.* A **458**, 2645.

BORKAR, A. & TSAMOPOULOS, J. 1991 Boundary-layer analysis of the dynamics of axisymmetric capillary bridges. *Phys. Fluids* A **3**, 2866.

CHEN, J. C., SHEN, J. C. & LEE, Y. T. 1990 Maximum stable length of nonisothermal liquid bridges. *Phys. Fluids* A **2**, 1118.

CHEN, Y.-J., ROBINSON, N. D., HERNDON, J. M. & STEEN, P. H. 1999 Liquid bridge stabilization theory guides a codimension-two experiment. *Comput. Meth. Appl. Mech. Engng* **170**, 209.

DIJKSTRA, H. A. 1993 On the shear stabilization of capillary breakup of finite liquid bridges. *Microgravity Sci. Tech.* **4**, 13.

DIJKSTRA, H. A. & STEEN, P. H. 1991 Thermocapillary stabilization of the capillary breakup of an annular film of liquid. *J. Fluid Mech.* **229**, 205.

DOEDEL, E. J. 1981 AUTO: A program for the automatic bifurcation analysis of autonomous systems. *Congressus Numerantum* **30**, 265. (*Proc. 10th Manitoba Conf. on Numerical Mathematics and Computation, University of Manitoba, Winnepeg, Canada, 1980.*)

EGGERS, J. & DUPONT, T. F. 1994 Drop formation in a one-dimensional approximation of the Navier–Stokes equation. *J. Fluid Mech.* **262**, 205.

GAUGLITZ, P. A. & RADKE, C. J. 1988 Extended evolution equation for liquid film breakup in cylindrical capillaries. *Chem. Engng Sci.* **437**, 1457.

GILLETTE, S. E. & DYSON, D. C. 1971 Stability of fluid interfaces of revolution between two equal circular plates. *Chem. Engng J.* **2**, 44.

GOLUBITSKY, M. & SCHAEFFER, D. G. 1985 *Singularities and Groups in Bifurcation Theory*, Vol 1. Springer.

GOLUBITSKY, M., STEWART, I. & SCHAEFFER, D. G. 1988 *Singularities and Groups in Bifurcation Theory*, Vol 2. Springer.

GUCKENHEIMER, J. 1986 Strange attractors in fluids: another view. *Annu. Rev. Fluid Mech.* **18**, 15.

HAMMOND, P. S. 1983 Nonlinear adjustment of a thin annular film of viscous fluid surrounding a thread of another within a circular cylindrical pipe. *J. Fluid. Mech.* **137**, 363.

HU, H. H., LUNDGREN, T. S. & JOSEPH, D. D. 1990 Stability of core-annular flow with a small viscosity ratio. *Phys Fluids* A **2**, 1945.

IOOSS, G. & JOSEPH, D. D. 1981 *Elementary Stability and Bifurcation Theory*. Springer.

Kuhlmann, H. C. & Rath, H. J. 1993 Hydrodynamic instabilities in cylindrical thermocapillary liquid bridges. *J. Fluid. Mech.* **247**, 247.

Mancebo, F. J., Nicolas, J. A. & Vega, J. M. 1998 Chaotic oscillations in a nearly inviscid, axisymmetric capillary bridge at 2:1 parametric resonance. *Phys. Fluids* **10**, 1088.

Mashayek, F. & Ashgriz, N. 1995 Nonlinear instability of liquid jets with thermocapilarity. *J. Fluid Mech.* **283**, 97.

Murphy, S. P., Hendrick, J. J., Martin, M. J., Grant, R. W. & Lind, M. D. 1987 Floating zone processing of indium in earth orbit. *Mat. Res. Soc. Symp. Proc.* **87**, 139.

Oron, A., Davis, S. H. & Bankoff, G. 1997 Long-scale evolution of thin liquid films. *Rev. Mod. Phys.* **69**, 931.

Plateau, J. A. F. 1873 *Statique Expérimentale et Théorique des Liquides Soumis aux Seules Forces Moléculaires.* Paris, Gauthier-Villars.

Raman, R. P. 1995 Numerical modeling of liquid encapsulated melt zone and a comparison with microgravity based experimental studies. MS thesis, University of Florida, Gainesville, FL.

Rayleigh, Lord 1879 On the capillary phenomena of jets. *Proc. R. Soc. Lond.* A **29**, 71.

Robinson, N. D. 2001 Experiments in film and liquid bridge dynamics and stability. PhD thesis, Cornell University.

Russo, M. J. & Steen, P. H. 1989 Shear stabilization of the capillary breakup of a cylindrical interface. *Phys. Fluids* A **1**, 1926.

Rybicki, A. & Floryan, J. M. 1987*a* Thermocapillary effects in liquid bridges: I. Thermocapillary convection. *Phys. Fluids* **30**, 1956.

Rybicki, A. & Floryan, J. M. 1987*b* Thermocapillary effects in liquid bridges. II. Deformation of the interface and capillary instability. *Phys. Fluids* **30**, 1973.

Saghir, M. Z., Abbaschian, R. & Raman, R. 1996 Numerical analysis of capillary convection in axisymmetric liquid encapsulated InBi. *J. Cryst. Growth* **169**, 110.

Stewart, I. 1981 Applications of catastrophe theory to the physical sciences. *Physica* D, 245.

Xu, J.-J. & Davis, S. H. 1985 Instability of capillary jets with thermocapilarity. *J. Fluid Mech.* **161**, 1.

Żolądek, H. 1984 On versality of a family of symmetric vector fields on the plane. *Math. USSR Sb.* **48**, 463.